Geodynamik, **70**.
Binder, D., Brückl, E., Roch, K.H., Behm, M., Schöner, W. & Hynek, B. (2009): Determination of total ice volume and ice-thickness distribution of two glaciers in the Hohe Tauern region, Eastern Alps from GPR data. - Annals of Glaciology, **50**(51): 71-79.
Brückl, E. (1970): Eine Methode zur Volumsbestimmung von Gletschern auf Grund der Plastizitätstheorie. - Archiv für Meteorologie, Geophysik und Bioklimatologie, Serie A **19**(3): 317-328.
Fischer, A. (2009): Calculation of glacier volume from sparse ice thickness data, applied to Schaufelferner, Austria. - Journal of Glaciology, **55** (191): 453-460.
Fischer, A., Span, N., Kuhn, M., Massimo, M. & Butschek, M. (2007): Radarmessungen der Eisdicke Österreichischer Gletscher. Band II: Messungen 1999 bis 2006. - Österreichische Beiträge zu Meteorologie und Geophysik, **39**: 142pp.
Lamprecht, A. & Kuhn, M. (2007): Glacier changes in the Austrian Alps during the last three decades, derived from the new Austrian glacier inventory. - Annals of Glaciology, **46**: 177-184.
Narod, B.B. & Clarke, G.K.C. (1994): Miniature high-power impulse transmitter for radio-echo sounding. - Journal of Glaciology, **40** (134): 190-194.
Rose, G.C. & Vickers, R.S. (1974): Calculated and experimental response of restively loaded V antennas to impulsive excitation. - Int. J. Electron., **37**: 261-271.
Span, N., Fischer, A., Kuhn, M., Massimo, M. & Butschek, M. (2005): Radarmessungen der Eisdicke österreichischer Gletscher, Band I: Messungen 1995 bis 1998. - Österreichische Beiträge zur Meteorologie und Geophysik, **33**: 146 pp.
Wu, T.T. & King, R.W.P. (1965): The cylindrical antenna with non-reflecting resistive loading, IEEE Trans. - Antennas Propag., **13**(3): 369-373.

Homogenization of 50 years of mass balance data at Hintereisferner, Austria

Fischer, A.[1] & Abermann, J.[1,2]

[1] Institut für Meteorologie und Geophysik der Universität Innsbruck, Innrain 52, 6020 Innsbruck, Österreich;
[2] Kommission für Geophysikalische Forschungen der Österreichischen Akademie der Wissenschaften, Innrain 52, 6020 Innsbruck, Österreich

The annually measured direct mass balance data of Hintereisferner was homogenized and analyzed with respect to climate and glacier changes. The spatial distribution of specific mass balance in the first decade of measurements was changed based on the measured data and according to the current methods and the concepts of modern mass balance analysis on Hintereisferner. This and the homogenization of the glacier area resulted in a better agreement with the results of the geodetic method.
The homogenized spatial distribution of the specific mass balance data was further analyzed with the aim to separate the influence of climate change from the effect of glacier changes. Therefore, the mass balance at three sub areas was compared to the total mass balance and to summer temperatures and winter precipitation measured at the nearby climate station in Vent. The mass balance at high elevations is determined by winter precipitation, the mass balance at low elevations by summer temperatures. Between 1953 and 2003, the surface of the glacier tongue lowered by 160 m. This resulted in a temperature increase of about 1 °C at the surface 2003 compared to the surface 1953 with the same temperature measured in Vent. The potential incoming solar radiation during the summer is reduced due to increased shading as a result of higher elevation differences between the glacier surface and the surrounding mountains. Comparing the effect of these two factors, the impact of the topographic temperature change on mass balance is much higher than the impact of decreased incoming radiation. At higher elevations, the effect of topographic changes is small compared to changes in the mean surface albedo.
The comparison of summer temperatures and precipitation measured in Vent to the specific mass balance showed that extremes in temperatures and precipitation do not coincide with extreme values of mass balance. Mean summer temperatures and mass balance are not directly coupled, since the occurrence of snow and ice melt and the extent of a temporal snow cover play important roles. Those are determined by the chronological sequence and duration of local weather conditions. The results of the degree-day method show that the increased glacier melt in the last decade is caused by an increase of positive degree day sums and a decrease of summer snow fall events.
All glacier related climate proxies as hydrological and direct mass balance as well as length measurements show the same trends, but differ in magnitude and in the processes and time scales comprised in the proxy. The comparison of the hydrological balance of the Rofenache basin to the direct mass balance data showed that Hintereisferner is not representative for all glaciers in the basin.

The not-so-simple effects of boundary conditions on models of simple shear

Frehner, M.[1], Exner, U.[1],
Mancktelow, N.N.[2] & Grujic, D.[3]

[1] Department of Geodynamics and Sedimentology, University of Vienna, Austria;
[2] Geological Institute, ETH Zurich, Switzerland;
[3] Department of Earth Sciences, Dalhousie University, Halifax, Canada

Analogue modeling of geological structures, such as the behavior of inclusions in a matrix or folding instabilities commonly employs a linear simple shear or general shear rig. In theory, a homogeneous plane strain flow is prescribed at the boundaries of such deformation rigs, but, in practice, the resulting internal deformation of the analogue material (commonly paraffin wax or silicone putties) often strongly deviates from the intended homogeneous strain field. This can easily lead to misinterpretation of such analogue experiments. We present a numerical finite element approach to quantify the influence of imperfect simple shear boundary conditions on the internal deformation of a homogeneous viscous analogue material. The results (Fig. 1) demonstrate that imperfect circumferential boundary conditions in the simp-

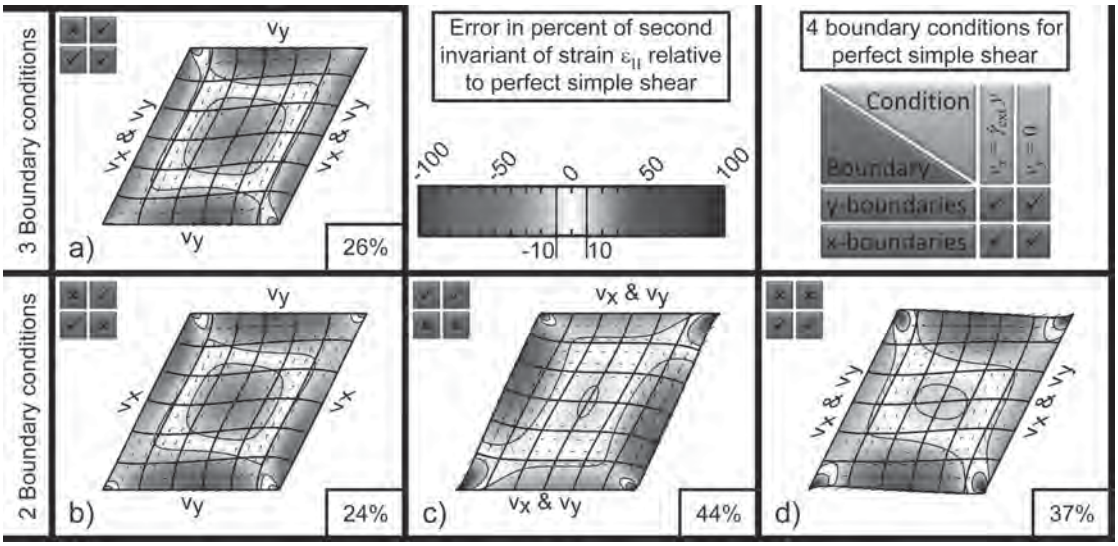

Fig. 1: Numerically deformed homogeneous square in simple shear with an applied shear strain of 0.5. For perfect simple shear (not shown here), four boundary conditions need to be applied, which are listed in the table in the upper right corner of the figure. In a), only three and in b) to d), only two boundary conditions are applied (indicated in each upper left corner in the same way as in the table and noted at each boundary). Thick black lines are passive marker lines. The color represents the second invariant of finite strain, plotted as the error in percent relative to perfect simple shear. Thin black lines are the ±10 % contour lines. Numbers in the lower right corner of each subfigure represents the area of the model with an absolute error smaller than 10 %. Arrows represent the scaled finite perturbation displacement, i.e. the difference between the actual displacement and perfect simple shear.

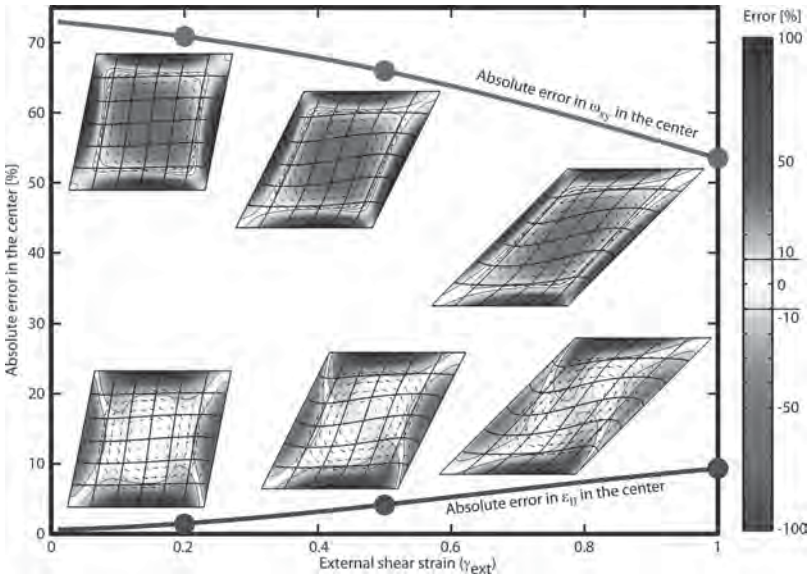

Fig. 2: Numerically deformed homogeneous square in simple shear with increasing applied shear strain and perfect simple shear boundary conditions in the *x*-*y*-plane, but viscous drag boundary conditions in the *z*-direction. In the inset figures, the color represents the second invariant of finite strain (lower inset figures) and the finite spin (upper inset figures), respectively, both plotted as the error in percent relative to perfect simple shear. Thin black lines are the ±10 % contour lines. Thick black lines are passive marker lines. Arrows represent the scaled finite perturbation displacement, i.e. the difference between the actual displacement and perfect simple shear. The bold blue and red line represent the second invariant of finite strain and the finite spin at the very center of the model, respectively with big dots indicating the external shear strain for which the inset figures are plotted.

le shear plane (*x*-*y*-plane) lead to the heterogeneous strain observed in some analogue experiments, depending on their design. However, in other experiments, the analogue material lies on top of a weak lubricating material (e.g., Vaseline) or is sandwiched between two such materials. These layers lead to a viscous drag force acting on the surface of the analogue material that represents imperfect simple shear boundary conditions in the third dimension (*z*-direction). For this experimental configuration, the numerical results (Fig. 2) show that the lubricating layers are responsible for the heterogeneous strain observed in analogue models. The resulting errors in internal strain can be as high as 100 % and these important boundary effects, which are difficult to avoid, must be considered when interpreting analogue simple shear experiments.